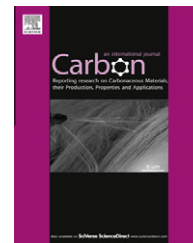


Available at [www.sciencedirect.com](http://www.sciencedirect.com)

SciVerse ScienceDirect

journal homepage: [www.elsevier.com/locate/carbon](http://www.elsevier.com/locate/carbon)

# Singly dispersed carbon nanotube/aluminum composites fabricated by powder metallurgy combined with friction stir processing

Z.Y. Liu, B.L. Xiao, W.G. Wang, Z.Y. Ma \*

Shenyang National Laboratory for Materials Science, Institute of Metal Research, Chinese Academy of Sciences, 72 Wenhua Road, Shenyang 110016, China

## ARTICLE INFO

### Article history:

Received 1 September 2011

Accepted 16 December 2011

Available online 23 December 2011

## ABSTRACT

Carbon nanotube (CNT)/aluminum composites were fabricated by a combination of powder metallurgy and subsequent friction stir processing (FSP). Microstructural observations indicated that the CNTs were singly dispersed in the composites. The CNTs tended to be dispersed along grain boundaries resulting in a much finer grain size. Although the CNTs were shortened and some  $Al_4C_3$  formed in the matrix, the layer structures of the CNTs were well retained. Raman spectroscopy also showed that the damage to CNTs during FSP was not severe. Compared to that of unreinforced Al, the yield strength of 1 wt.% and 3 wt.% CNT/Al composites increased by 23.9% and 45.0%, respectively. A strength equation relating with load transfer and the grain refinement was proposed to describe the increase of the yield strength of the composites.

© 2011 Elsevier Ltd. All rights reserved.

## 1. Introduction

Carbon nanotubes (CNTs), either single-walled (SWCNT) or multi-walled (MWCNT), have attracted much attention as the ideal reinforcements for composites because of their extremely high elastic modulus (around 1 TPa) and strength (30–100 GPa) as well as good thermal and electrical properties [1–5]. By incorporating the CNTs into appropriate matrixes, it is possible to produce the composites with enhanced properties. Although the main research efforts in the past decade were focused on the CNT reinforced polymer or ceramic matrix composites [6–8], a few groups have dedicated themselves to the fabrication of the CNT/metal composites, such as the aluminum matrix composites [9–11].

The dispersion of the CNTs in the metal matrix is a key challenge for fabricating the CNT/metal composites, because the entangled or bundled CNT clusters are easily induced as a result of their large aspect ratio and the strong Vander force. The entangled and bundled CNTs would reduce either

mechanical or physical properties of the composites reinforced with the CNTs. In the past few years, powder metallurgy (PM) route has been commonly used to fabricate the CNT/metal composites because it is easier to incorporate the CNTs into the metal matrix by PM than by casting processing, which has the problems of poor wetting properties and large density differences between CNTs and metal melt.

In the conventional PM route, the CNTs were usually pre-functionalized to reduce the entangled CNT clusters and thus improve the homogeneity degree of CNT dispersion in the metal matrix [10]. However, the functionalization of the CNTs inevitably opens either the ends or the sidewalls of the CNTs, disrupting the  $\pi$ -electron system and impairing electronic and thermal properties [12]. Furthermore, the reinforcement distribution in the metal matrix depends on the particle size ratio of metal powder to reinforcement powder [13,14]. Unfortunately, the size of available industrial metal powders is too large to be used in obtaining a homogeneous CNT distribution in the composites with high CNT concentrations. To overcome

\* Corresponding author. Fax: +86 24 83978908.

E-mail address: [zyrna@imr.ac.cn](mailto:zyrna@imr.ac.cn) (Z.Y. Ma).

0008-6223/\$ - see front matter © 2011 Elsevier Ltd. All rights reserved.

doi:10.1016/j.carbon.2011.12.034

this problem, the high energy ball mill (HEM) process has been used to fabricate the CNT/metal composite powders. During the HEM process, the CNTs could be uniformly distributed into the metal matrix due to repeated deformation, cold welding and fracturing processes of the metal powders. Unfortunately, the HEM process would contaminate the composite powders and cause severe damage to the CNTs because of its large energy input as well as the lengthy treatment time [15,16]. Therefore, developing a new route for fabricating the CNT/metal composite is highly desirable.

Friction stir processing (FSP), a development based on the basic principles of friction stir welding (FSW) [17], is a relatively new metal-working technique. The basic concept of FSP is remarkably simple. A non-consumable rotating tool with a specially designed pin and shoulder is inserted into a workpiece and traversed along the desired path to cover the region of interest (Fig. 1). The tool heats the workpiece via the friction between the tool and workpiece and by the plastic deformation of the material, and drives the softened material around the pin to flow. The combination of tool rotation and translation results in the movement of material from the front to the back of the pin. Thus, the material in the processed zone is severely deformed and thoroughly mixed in solid state, achieving localized microstructural modification for specific property enhancement.

FSP has been demonstrated to be an effective method of incorporating the reinforcing particles, e.g. nano-sized particles [18–20], into the metal matrix, and homogenizing the microstructure of heterogeneous materials, such as cast alloys and composites. Johannes et al. [21] and Morisada et al. [22] fabricated CNT/aluminum alloy composites using FSP. They inserted the CNTs into the holes or grooves which were pre-machined on the aluminum plates, and then subjected the plates to FSP. Their results demonstrated that the HV hardness of the aluminum alloys was increased after incorporating the CNTs by FSP. However, the tensile strengths of the CNT/metal composites were not reported. Furthermore, it was hard to accurately control the CNT concentration because not all CNTs in the holes or grooves could be mixed into the matrix.

In this work, a modified fabrication processing of the CNT/aluminum composites was used. First, 1 wt.% (1.5 vol.%) and 3 wt.% (4.5 vol.%) CNT reinforced Al–Cu–Mg composites were fabricated using a conventional PM process to form a bulk billet. The billet was then subjected to FSP to improve the distribution of the CNTs. The aim of this work is to establish an effective route of dispersing the CNTs into the aluminum alloy matrix. Furthermore, the relationship between microstructure and strength of the composites is also discussed.

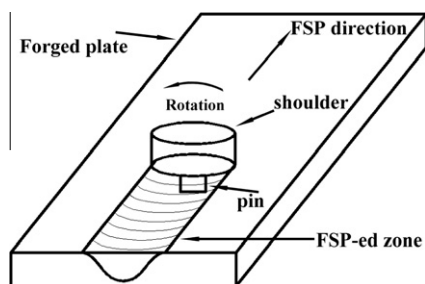


Fig. 1 – Schematic of friction stir processing (FSP).

## 2. Experimental

### 2.1. Raw materials and composite fabrication

As-received CNTs (95–98% purity) provided by Tsinghua University, had entangled morphologies with an outer diameter of 10–30 nm and a length of several microns (Fig. 2(a)). No extra pre-treatments were conducted on the CNTs. 1 wt.% and 3 wt.% CNTs were mixed with Al–4.5 wt.%Cu–1.2 wt.%Mg (2009Al) alloy powders, with an average diameter of 10  $\mu\text{m}$  (Fig. 2(b)), in a bi-axis rotary mixer running at 50 rpm for 8 h with a 1:1 ball to powder ratio. The as-mixed powders were cold-compacted in a cylinder die, degassed and hot-pressed into cylindrical billets with a diameter of 55 mm and a height of 50 mm.

The as-pressed billets were hot forged with steel canning at 723 K into disc plates with a thickness of about 10 mm. Then the plates were subjected to 1-pass or in situ 4-pass FSP (shown in Fig. 1) at a tool rotation rate of 1200 rpm and a travel speed of 100 mm/min (under this FSP parameter, a good dispersion effect of CNTs into the aluminum matrix could be obtained), using a tool with a concave shoulder 20 mm in diameter, a threaded cylindrical pin 6 mm in diameter and 4.2 mm in length. For comparison, unreinforced 2009Al was also fabricated under the same conditions. The as-FSP composites and 2009Al alloy were solutionized at 768 K for 2 h, water quenched, and then naturally aged for 4 days.

### 2.2. Characterization of the composites

The CNT distributions in the matrix under various fabrication conditions were examined using the optical microscopy (OM, Zeiss Axiovert 200MAT), scanning electron microscopy (Quanta 600), field emission scanning electron microscopy (Leo Supra) and transmission electron microscopy (Tecnai G2 20). Raman spectroscopic measurements were conducted using the JY Labram HR 800 (excitation about 1  $\mu\text{m}$ ). The densities of the composites were determined using the Archimedeian principle. Distilled water was used as the liquid for the measurement and at least three samples were tested to obtain accurate average value. The Vickers microhardness (HV) of the materials was measured using a Leco-LM-247 AT indenter under a load of 1000 g for 30 s.

Tensile specimens with a gauge length of 2.5 mm, a width of 1.5 mm and a thickness of 0.8 mm were machined from the FSP composites perpendicular to the FSP direction. Tensile tests were conducted at a strain rate of  $1 \times 10^{-3} \text{ s}^{-1}$  at room temperature. For comparison, the tensile test of the 2009Al and the forged composites were also conducted under the same conditions.

## 3. Results

### 3.1. CNT distribution

Fig. 3 shows the cross-sectional macrographs of the FSP composites and the hardness profiles along the mid-depth of the processed zone (PZ). After 1-pass FSP, the PZ was not asymmetrical, especially for 1 wt.% CNT/2009Al composite. However,

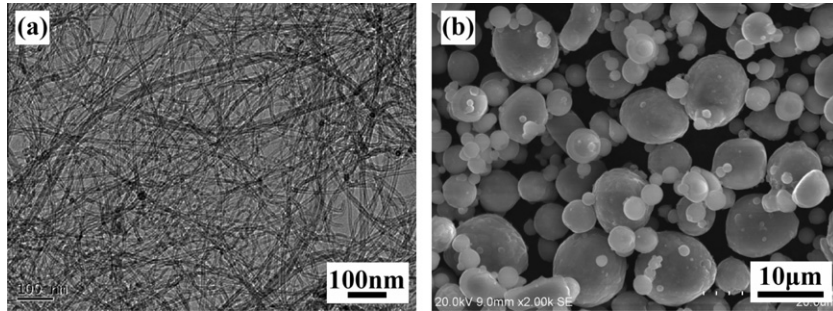


Fig. 2 – Morphology of the as-received (a) CNTs and (b) 2009Al powders.

after 4-pass FSP, basically symmetric and uniform PZs were produced for both 1 wt.% and 3 wt.% CNT/2009Al composites. The HV hardness values of the PZs were relatively uniform throughout the whole PZ, which also indicated that the PZs were basically symmetric and uniform. Furthermore, the hardness of the PZs was significantly increased compared with that of the forged composites.

Figs. 4 and 5 show the CNT distributions in 1 wt.% and 3 wt.% CNT/2009Al composites under different conditions, respectively. For the forged composites (Figs. 4(a) and 5(a)), obvious CNT clusters were observed. This is understandable, as the as-received CNTs were entangled with each other and the mixing and forging processes were not effective enough to disperse the CNTs into the aluminum matrix. Also, nearly no aluminum could be observed in the clusters because the CNTs could hardly be soaked by aluminum. After 1-pass FSP, the large CNT clusters were significantly reduced, leaving only much smaller clusters (Figs. 4(b) and 5(b)). Especially, alternate particle-poor zone and particle-rich zone were observed in the 1-pass FSP 3 wt.% CNT/2009Al compos-

ite (Fig. 5(b)). This banded structure resulted from complicated material flow during FSP. When the pin rotated one circle, one layer material was extruded downward along the pin wall. After the pin ran away, one particle-poor zone and one particle-rich zone were formed. However, after 4-pass FSP, neither the small clusters, nor the particle-poor/particle-rich zones could be found, at least under the OM and SEM (Figs. 4(c) and 5(c)). This indicates that the entangled CNTs were completely broken up and dispersed into the aluminum matrix due to intense stirring effect of the rotating threaded pin during FSP.

TEM observations revealed that the CNTs could be singly dispersed in the aluminum matrix of the 3 wt.%CNT/2009Al composite (Fig. 6). Furthermore, the CNTs in the composite were shorter than the as-received ones due to significant stirring and breakup during FSP, which was in accordance with the results of SiC whisker reinforced composites processed by other plastic deformation methods [23]. The shear effect during FSP first cut off the entangled CNTs and the fragments were subsequently dispersed into the aluminum matrix due

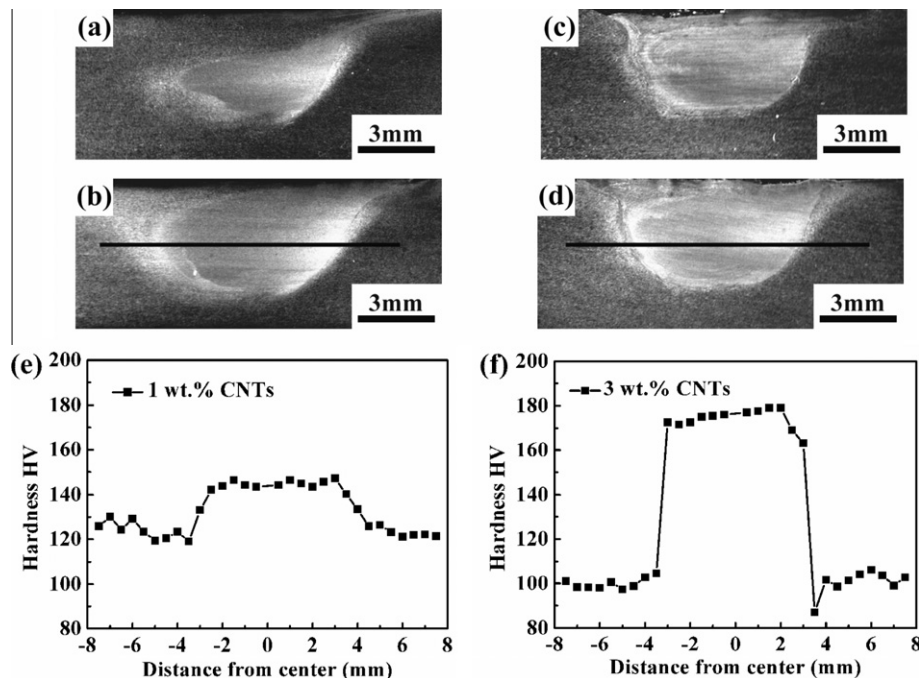


Fig. 3 – OM images of FSP CNT/2009Al composites: (a) 1 pass FSP, 1 wt.% CNT, (b) 4 pass FSP, 1 wt.% CNT, (c) 1 pass FSP, 3 wt.% CNT, (d) 4 pass FSP, 3 wt.% CNT; hardness profiles of FSP composites: (e) 4 pass FSP, 1 wt.% CNT, (f) 4 pass FSP, 3 wt.% CNT.

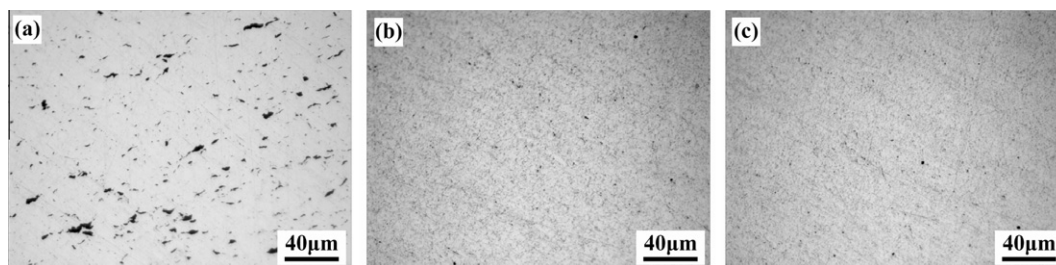


Fig. 4 – OM images showing CNT distribution in 1 wt.% CNT/2009Al composites: (a) forged, (b) 1-pass FSP, and (c) 4-pass FSP.

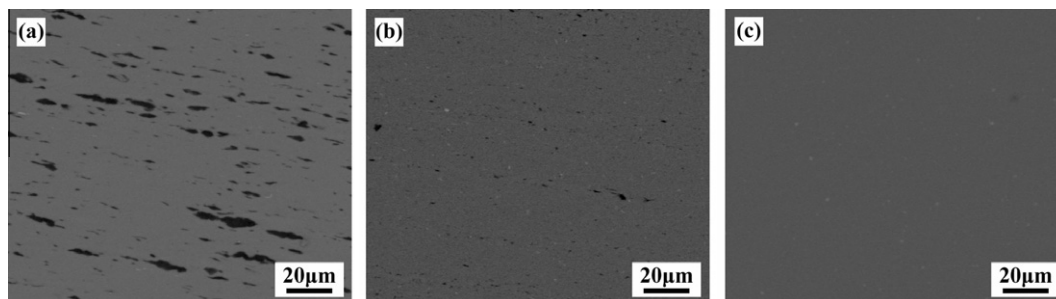


Fig. 5 – SEM images showing CNT distribution in 3 wt.% CNT/2009Al composites: (a) forged, (b) 1-pass FSP, and (c) 4-pass FSP.

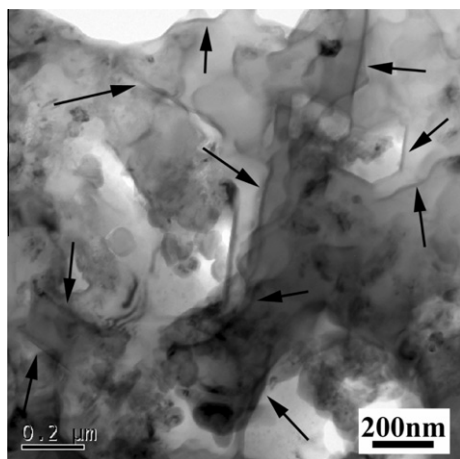


Fig. 6 – TEM image showing singly dispersed CNTs in 4-pass FSP 3 wt.% CNTs/2009Al composite.

to the plastic flow of the aluminum. After 4-pass FSP, the length of CNTs could still remain larger than 400 nm (Fig. 6).

Fig. 7 shows the grain microstructure of the FSP 2009Al alloy and CNT/2009Al composites. Significantly refined grain sizes were commonly observed in the FSP materials, such as aluminum alloys and magnesium alloys [24,25], due to the occurrence of dynamic recrystallization. It seemed that FSP pass had little influence on the grain size of the 2009Al alloy. Both the 1-pass and 4-pass FSP 2009Al had an average grain size of about 4 µm (Fig. 7(a) and (d)). By comparison, the FSP composites had a much finer grain size. After 1-pass FSP, the average grain size of 1 wt.% and 3 wt.% CNT/2009Al composites was of ~3 and 2 µm, respectively, (Fig. 7(b) and (c)), based on the TEM observations (about 50 grains were

counted). After 4-pass FSP, the average grain size of the 1 wt.% and 3 wt.% CNT/2009Al composites was of ~1.8 and 0.8 µm, respectively, (Fig. 7(e) and (f)), based on the TEM examinations (about 50 grains were counted). It indicated that the grain size decreased as the CNT concentration increased. Some of the grains, on the boundaries of which CNTs were found as shown by the inset in Fig. 7(f), were even finer. This is attributed to effective pinning effect of the nano-sized CNTs on the grain boundaries, which hindered the growth of the recrystallized grains during FSP. Thus, the grains in the composites showed a much finer size compared with those in the 2009Al alloy, and the grain size of the composites became finer as the FSP pass increased because more CNTs were dispersed in the aluminum matrix.

### 3.2. Damage to CNTs

To assess the damage to the CNTs during FSP, Raman spectroscopic measurements were carried out. The analysis areas in the forged composites and the 1-pass FSP composites were at the clusters, whereas the analysis areas for the 4-pass FSP composites were selected at random because the CNTs were distributed uniformly. The wavenumber corresponding to 1350 and 1600  $\text{cm}^{-1}$  represents the D-band and G-band of the CNTs, respectively. The intensity ratio of the D-band to G-band ( $I_D/I_G$ ) represents the degree of defects in the CNTs.

Fig. 8 shows that the  $I_D/I_G$  increased only a little with an increase in the number of FSP passes. The decreasing intensities of the  $I_D$  and  $I_G$  might result from different CNT numbers in the analysis areas. These results verified that FSP did not produce a significant effect on the structure of the CNTs, though FSP dispersed the CNTs into the Al matrix by intense plastic deformation. This might be due to a short

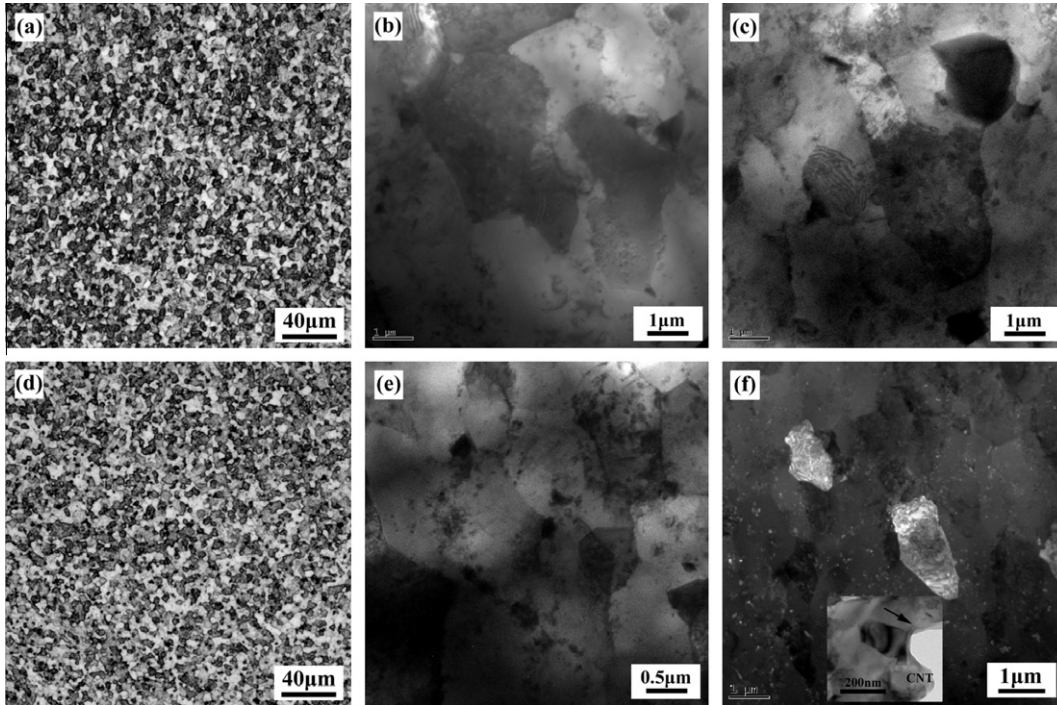


Fig. 7 – Grain structures of FSP samples: (a) 1-pass 2009Al (OM), (b) 1-pass 1 wt.% CNT/2009Al, (c) 1-pass 3 wt.% CNT/2009Al and (d) 4-pass 2009Al (OM), (e) 4-pass 1 wt.% CNT/2009Al, (f) 4-pass 3 wt.% CNT/2009Al (TEM, dark field image).

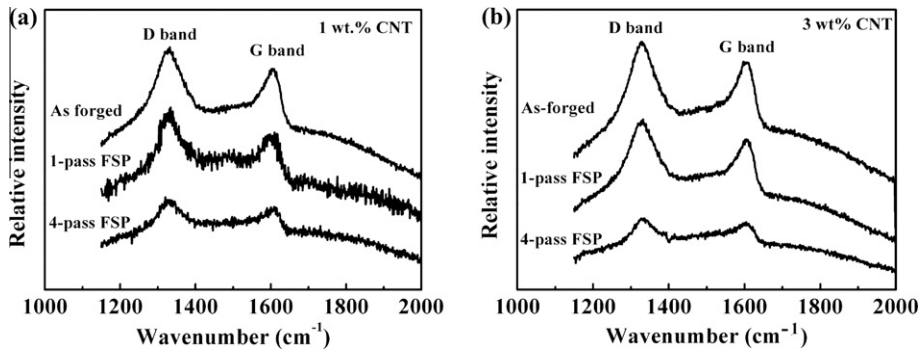


Fig. 8 – Raman spectra of CNT/2009Al composites with (a) 1 wt.% CNT, (b) 3 wt.% CNT.

application time and relatively low applied energy during FSP, compared to the high energy ball mill processing [26].

Fig. 9 shows the XRD patterns of the 3 wt.% CNT/2009Al composites. It is important to notice the presence of Al<sub>4</sub>C<sub>3</sub>, even in the forged composite. This indicates that the reaction between the CNTs and Al matrix occurred during fabrication. It is well documented that many defects commonly existed in MWCNTs [27]. The carbon atoms at these defected locations reacted easily with Al at high temperature. After 4-pass FSP, the peak of the Al<sub>4</sub>C<sub>3</sub> was increased. This is attributed to two factors. Firstly, significant shortening of the CNTs during FSP increased the number of carbon atoms at the tips of the CNTs, thereby increasing the intensity of the reaction between CNTs and Al matrix. Secondly, severe plastic deformation and high temperature during FSP promoted the CNT-Al reaction further.

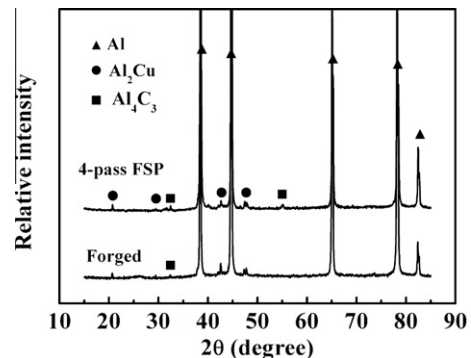


Fig. 9 – XRD patterns of 3 wt.% CNT/2009Al composites.

Fig. 10 shows the fine microstructure of the interfacial regions in the 3 wt.% CNT/2009Al composite after 4-pass FSP. It was noted that most of the interfaces between the CNT wall and the Al matrix were zigzagged but clean without reaction (Fig. 10(a)). However, the  $\text{Al}_4\text{C}_3$  could be found in the composite (Fig. 10(b) and (c)). They were attached to the CNTs or in the matrix near the CNTs. The sizes of the  $\text{Al}_4\text{C}_3$  were within 10–50 nm. The temperature during the composite fabrication was relatively low, with the maximum value of 560 °C in hot pressing. It is thought that a number of the defect sites existed in the as-received CNTs and FSP further increased the number of defect sites because the CNTs were cut short. Thus, the  $\text{Al}_4\text{C}_3$  formed in the defect sites during the composite fabrication. However, most of the layer structures (inter-layer distance about 0.324 nm) of the CNT walls were still well retained (Fig. 10(d)).

### 3.3. Mechanical properties of CNT/2009Al

Table 1 shows the densities and tensile properties of the composites. The densities of the composites increased with increasing the numbers of the FSP pass for both 1 wt.% and 3 wt.% CNT/2009Al composites. This is in accordance with the OM and SEM observations. As shown in Figs. 4 and 5, the CNT clusters and porosity ratio decreased as the number of FSP pass increased, which led to increased composite densities.

The yield strength (YS) and the ultimate tensile strength (UTS) of both forged 1 wt.% and 3 wt.% CNT/2009Al composites were much lower, even lower than those of the forged

2009Al alloy. Increasing the CNT concentration from 1 wt.% to 3 wt.% led to further decrease in both strength and elongation. In particular, the forged 3 wt.% CNT/2009Al composite exhibited a very low elongation of 1%, which is mainly attributed to a great number of large CNT clusters and voids in the clusters. After 1-pass FSP, the strengths of both 1 wt.% and 3 wt.% CNT/2009Al composites were improved significantly compared with those of the forged composites. Increasing the number of FSP pass from 1 to 4 resulted in a further strength increase for the CNT/2009Al composites, which was attributed to the further improved distribution of the CNTs in the aluminum matrix, but there was no obvious strength change for the 2009Al. The elongation of the 1 wt.% CNT/2009Al composite changed little with increasing the FSP pass, however, the 3 wt.% CNT/2009Al composite exhibited a gradually increasing elongation as the number of FSP pass increased.

It is noted that under the forged condition, increasing the CNT weight fraction from 1% to 3% resulted in a decrease in the YS. However, under the FSP conditions (both 1-pass and 4-pass FSP), increasing the CNT weight fraction from 1% to 3% resulted in an increase in the YS. Compared with that of the 4-pass FSP 2009Al alloy, the YS increased by about 23.9% and 45% for the 4-pass FSP 1 wt.% and 3 wt.% CNT/2009Al composites, respectively. Many references [10,28,29] reported that the YS began to decrease as the CNT concentrations increased to a critical value (commonly smaller than 1 wt.%). However, in this study, the YS could still increase as the CNT concentration increased to as high as 3 wt.%. This

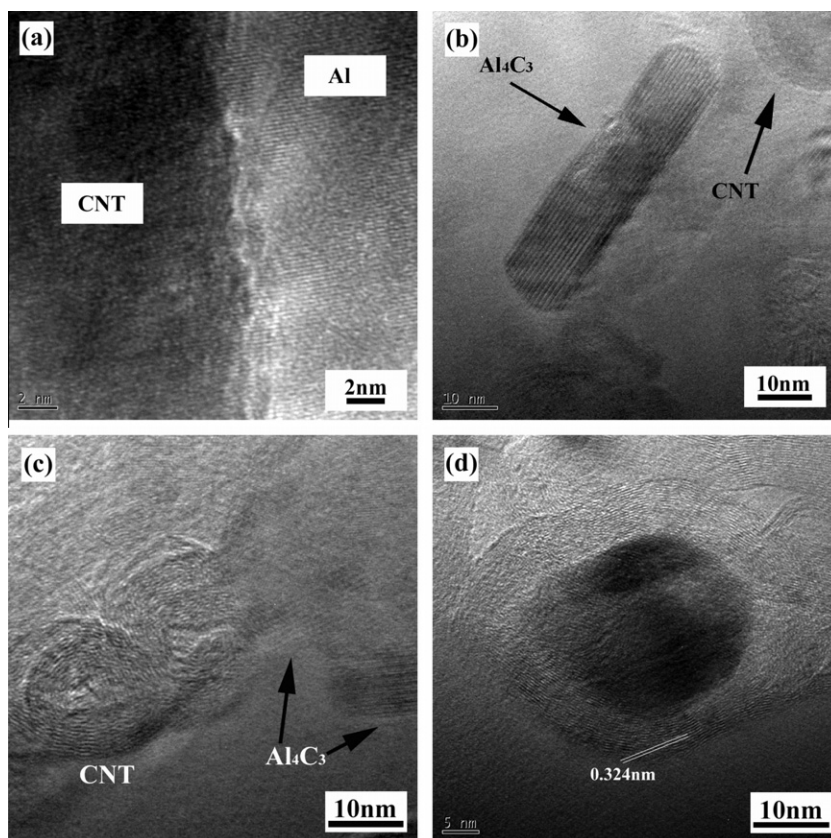


Fig. 10 – HREM images showing (a) interface between Al and CNT, (b)  $\text{Al}_4\text{C}_3$  in Al matrix near CNT, (c)  $\text{Al}_4\text{C}_3$  attached to CNT, and (d) layer wall structure of CNTs in 4-pass FSP 3 wt.% CNT/2009 Al composite.

**Table 1 – Densities and tensile properties of 2009Al and CNT/2009Al composites.**

Specimen		Density (g/cm <sup>3</sup> )	YS (MPa)	UTS (MPa)	El. (%)
2009Al alloy	Forged	2.757	299	411	12
	1-Pass FSP	2.755	297	421	13
	4-Pass FSP	2.760	305	417	15
1 wt.% CNT/2009Al	Forged	2.718	307	392	8
	1-Pass FSP	2.724	371	451	7
	4-Pass FSP	2.733	385	477	8
3 wt.% CNT/2009Al	Forged	2.642	273	298	1
	1-Pass FSP	2.679	414	437	2
	4-Pass FSP	2.704	435	466	4

is mainly attributed to the homogeneous dispersion of the CNTs in the aluminum matrix, the proper aspect ratio of the CNTs, and significant matrix grain refinement.

However, the UTS did not exhibit a similar variation tendency. Increasing the CNT weight fraction from 0% to 1% led to an increase in the UTS; however, the UTS began to decrease when the CNT weight fraction was increased further from 1% to 3%. Another noteworthy phenomenon was that the increase of the UTS for the FSP composites was not as obvious as that of the YS. Compared with the FSP 2009Al, the maximum UTS increase for the 1-pass and 4-pass FSP 1 wt.% CNT/2009Al composites was only 7.4% and 13%, respectively.

Although the CNTs were uniformly dispersed into the 2009Al matrix after 4-pass FSP, the elongations of the 1 wt.% and 3 wt.% CNT/2009Al composites were still lower than that of the 2009Al alloy. This is attributed to the fracture mode of the composite. The composite fracture is directly related to the reinforcement cracking and interfacial failure. For the composites with high fraction of reinforcements, voids tend to form at low strains during tension due to the stress concentration at the reinforcement-matrix interfaces, resulting in a low level of elongation.

Fig. 11 shows SEM fractographs of the 4-pass FSP 3 wt.% CNT/2009Al composite and 2009Al alloy. The 2009Al alloy showed deep and large dimples on the fracture surface (Fig. 11(c)), corresponding to larger elongation (Table 1), whereas the composite showed shallower and smaller dimples (Fig. 11(a)). Furthermore, uniformly distributed CNTs were observed on the fracture surfaces of the composite (Fig. 11(a)) and they were found to be the pulled out CNTs in the inners of the dimples under higher magnification (Fig. 11(b)).

For the composites reinforced with short fiber or whisker, an applied force can be transferred from the matrix to the reinforcement by a shear stress that is developed along the fiber/matrix interface. Thus, it generates a variation in stress along the fiber length; the stress on the fiber increases proportionally from the fiber end to reach a critical value at the mid-region when the fiber length is larger than the critical length ( $l_c$ ) defined as [30].

$$l_c = \frac{\sigma_f}{\sigma_{my}} d_f \quad (1)$$

where  $\sigma_{my}$  is the strength of the matrix,  $\sigma_f$  is the strength of the fiber and  $d_f$  is the average diameter of the fibers. The calculated  $l_c$  for the CNT/2009Al composite is about 1.5  $\mu\text{m}$ ,

which is much larger than the average CNT length ( $\sim 400$  nm). This means that the stress on the CNTs could not reach to the fracture strength of the CNTs. Thus, the CNTs on the fracture surfaces (Fig. 10(b)) might be directly pulled out from the matrix. Considering the damage of the CNTs, it is also possible for some CNTs to be broken before pulled out from the matrix. This indicates that the length of the CNTs was not large enough to be compatible with the high strength of the CNTs. It might be one possible reason why the UTS of the composites were not increased as highly as the YS.

#### 4. Strength improvement by CNT incorporation

Three possible strengthening mechanisms for the CNT/metal composites had been discussed by George and Kashyap [9], namely the thermal mismatch, Orowan looping and shear lag models. The elastic modulus of the composites was in accordance with the value calculated by the shear lag model. However, none of the mentioned models were able to predict the YS changes of the composites. A main reason was the presence of the CNT clusters. For the FSP CNT/2009Al composites, the CNTs were singly dispersed in the matrix, which made the strength discussion possible.

To predict the strength of the composites, the modified shear lag model developed by Nardone and Prewo [31] is perhaps the most classic one. It suits for the composites reinforced by short fiber or whisker when the lengths of the reinforcement were shorter than critical length which was described in Eq. (1). In the modified shear lag model, the load transfer from the matrix to the reinforcements through not only the principal tensile stress but also the shear stress. According to the modified shear lag model, the strength of the composites may be calculated by [31]:

$$\sigma_c = \sigma_m [V_f(s+4)/4 + (1 - V_f)] \quad (2)$$

where  $\sigma_c$  and  $\sigma_m$  are the yield strength of the composite and matrix, respectively;  $s$  is the aspect ratio of the CNTs, and  $V_f$  is the volume fraction of the CNTs.

It should be noted that the grain size was significantly refined due to the existence of the CNTs dispersed in the matrix. Grain refinement is another reason for the YS increase according to the Hall–Petch relationship [11], which could be expressed by:

$$\sigma_m = \sigma_0 + kd^{-1/2} \quad (3)$$

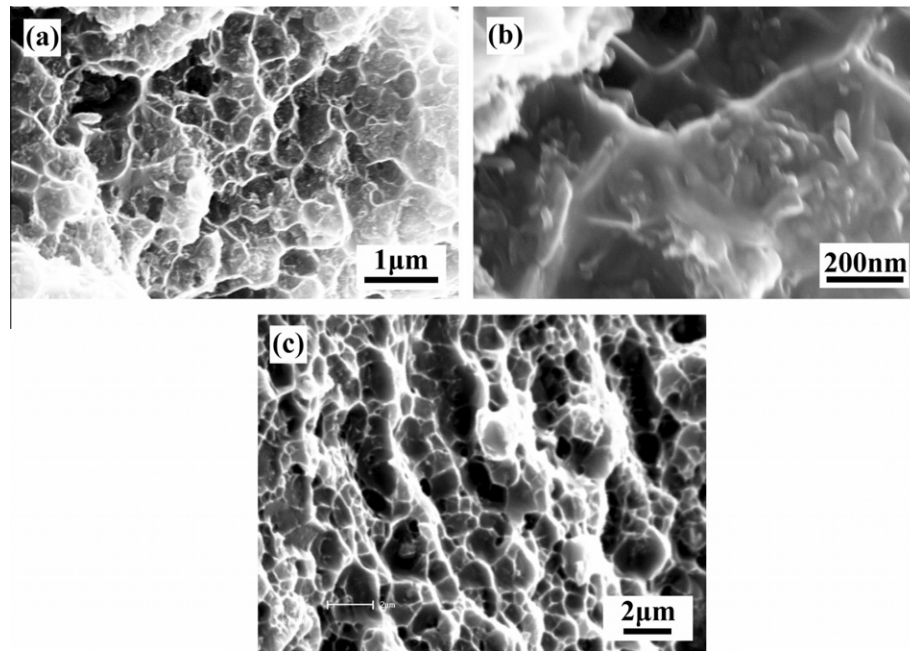


Fig. 11 – SEM fractographs of (a) 4-pass FSP 3 wt.% CNT/2009Al composite, (b) a magnified image showing CNTs on fracture surface, and (c) 4-pass FSP 2009Al.

Table 2 – Experimental and calculated YS of CNT/metal composites.

Matrix	CNT content	d (nm)	s	Experimental YS (MPa)	Calculated YS (MPa)	Ref.
2009Al	0 wt.%	4000	–	300 ± 6	–	This study
	1 wt.%	1800	20	385 ± 7	372	
	3 wt.%	800	20	435 ± 11	452	
Pure Al	0 vol.%	72	–	350	–	[11]
	4 vol.%	70	28.6	410	429	
	4 vol.%	200	28.6	320	308	
Co	0 vol.%	2000	–	700	–	[33]
	7 vol.%	310	33.3	1500	1537	

where  $\sigma_0$  is rationalized as either a frictional stress to the motion of dislocation glide or an internal back stress,  $d$  is the matrix grain size in the composite, and  $k$  is the Hall–Petch slope, for Al–Cu–Mg alloy it is about 0.1 MPa m<sup>1/2</sup> [32].

Orowan looping strengthening was the main strengthening mechanism for the fine particle/metal composites, however it could be ignored because the CNTs were mainly dispersed along the grain boundaries of the aluminum matrix as shown in Fig. 7(f). Further, the number of the Al<sub>4</sub>C<sub>3</sub> formed during fabrication was quite few and most of them were attached to the CNT as shown by HREM examinations (Fig. 10(c)), therefore the effect of the Al<sub>4</sub>C<sub>3</sub> could be ignored in our calculations. Thus, the yield strength of the composites could be expressed by:

$$\sigma_c = (\sigma_0 + kd^{-1/2})[V_f(s+4)/4 + (1 - V_f)] \quad (4)$$

In this study, the aspect ratio of the CNTs is about 20 (diameter 10–30 nm, effective length about 400 nm) and the effective length of the CNTs is smaller than the critical length

(about 1.5 μm), which means that the YS calculation based on Eq. (4) is reasonable. The YS of the matrix with the grain size of 4 μm is 300 MPa. The used grain sizes for the 1 wt.% and 3 wt.% CNT/2009Al composites were 1800 and 800 nm, respectively. The calculated YS of the 4-pass FSP 1 wt.% and 3 wt.% CNT/2009Al composites are compared with experimental results in Table 2. It is noted that the calculated YS by Eq. (4) are in good agreement with the experimental values. For the 1 wt.% and 3 wt.% CNT/2009Al composites, the deviations between the experimental and calculated strengths are only 3.4% and 3.8%, respectively. Thus, Eq. (4) could explain the YS increasing phenomenon, which also indicated that the load transfer mechanism and Hall–Petch relationship dominate the YS increase in the FSP CNT/Al composites.

To verify Eq. (4) further, the YS data from Refs. [11,33] were also introduced. In these composites, the CNTs were found to be uniformly distributed in the matrix. The CNT/Al composites in Ref. [11] (high energy ball milled and then extrusion processed) had a pure aluminum matrix and the CNTs with

an aspect ratio of  $\sim 28.6$  (diameter about 35 nm, length about 1  $\mu\text{m}$ ), and the effective length of the CNTs is smaller than the critical length (about 3.7  $\mu\text{m}$ ), which qualifies the YS calculation based on Eq. (4).  $k$  and  $\sigma_0$  are 2000 MPa nm<sup>1/2</sup> and 98 MPa, respectively, from Ref. [11]. The calculated and experimental YS results are listed in Table 2. The discrepancies between the experimental and calculated results are 4.6% and 3.8% for the CNT/Al composites with grain size of 72 and 200 nm, respectively.

The CNT/Co composite in Ref. [33] was fabricated by molecular mixing methods. The CNTs had an aspect ratio of 100. Considering that the CNTs were randomly oriented in the matrix, the effective aspect ratio (about 33.3) was obtained using the method which was used for calculating the effective aspect ratio of SiC whiskers from Ref. [23]. And the effective CNT length of  $\sim 600$  nm and the critical length of 620 nm were at the same level, thus the yield strength calculation based Eq. (4) is reasonable. The calculated and experimental YS results are shown in Table 2. The discrepancy between the experimental and calculated results is 2.3%. It could be concluded that the calculated YS are in good agreement with the experimental YS, which also indicates that both grain refinement and load transfer contribute to the YS increase.

The increase of the UTS in short fiber or whisker/metal composites could be partly attributed to the load transfer mechanism. The CNTs have much high strength, thus interface debonding or failure of the matrix near the interface were two main failure modes for the CNT/metal composites, which was evidenced by SEM fractography (Fig. 10(b)). For the present FSP composites, the CNTs aligned randomly in the matrix, which means that the stress on the CNT interfaces was quite different. The interfacial stress on the CNTs which aligned along the tensile axis was much larger, thus the CNTs were prone to failing earlier than other oriented CNTs. This could be reflected by comparing our tensile strength with that of Deng's [34]. The CNTs in as-extruded 1 wt.% CNT/2024Al composite had a similar orientation and therefore they had much similar interfacial stress level and tended to debond synchronously during tension [34]. Thus, though the YS of as-extruded 1 wt.% CNT/2024Al (336 MPa) was much lower than that of the present FSP composite, the UTS (471 MPa) was similar to that of the FSP composite.

Furthermore, a large stress concentration appeared at the tips of the CNTs during tension, however the matrix around the CNTs had much smaller ability to be hardened due to the existence of the CNTs. Thus, during the tension, the stress of the matrix near the tips of the CNTs became much larger because it could be hardly relaxed, resulting in the initiation of the crack. As a result, the increase of the UTS is not as high as that of the YS. Compared with the 1 wt.% CNT/2009Al, the 3 wt.% CNT/2009Al had smaller interparticle spacing between the CNTs, which means that the stress near the CNT tips was more difficult to be relaxed. Thus, the interfaces in the 3 wt.% CNT/2009Al more easily failed, and therefore, the UTS of the 3 wt.% CNT/2009Al was even a little lower than that of the 1 wt.% CNT/2009Al.

## 5. Conclusions

- (1) FSP could break down the CNT clusters and disperse the CNTs into the matrix, and the distribution homogenization of the CNTs increased with increasing FSP pass. The single dispersion of the CNTs was achieved in the 4-pass FSP CNT/2009Al composites with most of the CNTs being distributed along the grain boundaries.
- (2) The CNTs in the composites were shortened compared to the as-received ones, but still remained larger than 400 nm. Al<sub>4</sub>C<sub>3</sub> were detected to attach to the CNTs or be in the matrix near the CNTs. However, the layer structures of the CNTs were still retained. The grain size of the FSP CNT/2009Al composites was significantly refined compared with that of the FSP 2009Al.
- (3) The mechanical strengths of the FSP CNT/2009Al composite, especially the YS, showed substantial improvements compared with the FSP 2009Al. Increasing the CNT concentration from 0 to 3 wt.% resulted in the increase in the YS. The UTS increased with increasing the CNT concentration from 0 to 1 wt.%, however it decreased as the CNT concentration increased up to 3 wt.%.
- (4) A YS equation based on the load transfer and grain refinement was proposed to predict the YS of the CNT/2009Al composites. The predicted results were in good agreement with the experimental results. This indicates that the YS increase of the CNT/2009Al composites is attributed to the load transfer from the matrix to the CNTs and the grain refinement.

## Acknowledgements

The authors gratefully acknowledge the support of (a) the National Research Program of China under grant no. 2011CB932603 and (b) the National Natural Science Foundation of China under grant no. 50890171.

## REFERENCES

- [1] Krishnan A, Dujardin E, Ebbesen TW, Yianilos PN, Treacy MMJ. Young's modulus of single-walled nanotubes. *Phys Rev B* 1998;58(20):14013–9.
- [2] Wong EW, Sheehan PE, Lieber CM. Nanobeam mechanics: elasticity, strength, and toughness of nanorods and nanotubes. *Science* 1997;277(5334):1971–5.
- [3] Salvétat-Delmotte J-P, Rubio A. Mechanical properties of carbon nanotubes: a fiber digest for beginners. *Carbon* 2002;40(10):1729–34.
- [4] Poncharal P, Wang ZL, Ugarte D, De WA. Electrostatic deflections and electromechanical resonances of carbon nanotubes. *Science* 1999;283(5407):1513–6.
- [5] Qian D, Wagner GJ, Liu WK, Yu M-F, Ruoff RS. Mechanics of carbon nanotubes. *Appl Mech Rev* 2002;55(6):495–533.
- [6] Curtin WA, Sheldon BW. CNT-reinforced ceramics and metals. *Mater Today* 2004;7(11):44–9.

- [7] Kim YA, Hayashi T, Endo M, Gotoh Y, Wada N, Seiyama J. Fabrication of aligned carbon nanotube-filled rubber composite. *Scr Mater* 2006;54(1):31–5.
- [8] Ahmad I, Unwin M, Cao H, Zhu YQ. Multi-walled carbon nanotubes reinforced Al<sub>2</sub>O<sub>3</sub> nanocomposites: mechanical properties and interfacial investigations. *Compos Sci Technol* 2010;70(8):1199–206.
- [9] George R, Kashyap KT. Strengthening in carbon nanotube/aluminium (CNT/Al) composites. *Scr Mater* 2005;53(10):1159–63.
- [10] Deng CF, Wang DZ. Processing and properties of carbon nanotubes reinforced aluminum composites. *Mater Sci Eng A* 2007;444(1–2):138–45.
- [11] Choi HJ, Kwon GB, Lee GY, Bae DH. Reinforcement with carbon nanotubes in aluminum matrix composites. *Scr Mater* 2008;59(3):360–3.
- [12] Banerjee S, Hemraj-Benny T, Won SS. Covalent surface chemistry of single-walled carbon nanotubes. *Adv Mater* 2005;17(1):17–29.
- [13] Liu ZY, Wang QZ, Xiao BL, Ma ZY, Liu Y. Experimental and modeling investigation on SiCp distribution in powder metallurgy processed SiCp/2024 Al composites. *Mater Sci Eng A* 2010;527(21–22):5582–91.
- [14] Liu ZY, Wang QZ, Xiao BL, Ma ZY. Clustering model on the tensile strength of PM processed SiCp/Al composites. *Composites Part A* 2010;41(11):1686–92.
- [15] Esawi A, Morsi K. Dispersion of carbon nanotubes (CNTs) in aluminum powder. *Composites Part A* 2007;38(2):646–50.
- [16] Kwon H, Park DH, Silvain JF, Kawasaki A. Investigation of carbon nanotube reinforced aluminum matrix composite materials. *Compos Sci Technol* 2010;70(3):546–50.
- [17] Mishra RS, Ma ZY. Friction stir welding and processing. *Mater Sci Eng R* 2005;50:1–78.
- [18] Berbon PB, Bingel WH, Mishra RS, Bampton CC, Mahoney MW. Friction stir processing: a tool to homogenize nanocomposite aluminum alloys. *Scr Mater* 2001;44(1):61–6.
- [19] Mishra RS, Ma ZY, Charit I. Friction stir processing: a novel technique for fabrication of surface composite. *Mater Sci Eng A* 2003;341(1–2):307–10.
- [20] Morisada Y, Fujii H, Nagaoka T, Fukusumi M. Nanocrystallized magnesium alloy-uniform dispersion of C<sub>60</sub> molecules. *Scr Mater* 2006;55(11):1067–70.
- [21] Johannes LB, Yowell LL, Sosa E, Arepalli S, Mishra RS. Survivability of single-walled carbon nanotubes during friction stir processing. *Nanotechnology* 2006;17(12):3081–4.
- [22] Morisada Y, Fujii H, Nagaoka T, Fukusumi M. MWCNTs/AZ31 surface composites fabricated by friction stir processing. *Mater Sci Eng A* 2006;419(1–2):344–8.
- [23] Hong SH, Chung KH, Lee CH. Effects of hot extrusion parameters on the tensile properties and microstructure of SiC<sub>w</sub>-2124 Al composites. *Mater Sci Eng A* 1996;206(2):225–32.
- [24] Feng AH, Ma ZY. Enhanced mechanical properties of Mg–Al–Zn cast alloy via friction stir processing. *Scr Mater* 2007;56(5):397–400.
- [25] Mishra RS, Ma ZY. Friction stir welding and processing. *Mater Sci Eng R* 2005;50(1–2):1–78.
- [26] Poirier D, Gauvin G. Structural characterization of a mechanically milled carbon nanotube/aluminum mixture. *Composites Part A* 2009;40(9):1482–9.
- [27] Andrews R, Jacques D, Qian D, Dickey EC. Purification and structural annealing of multiwalled carbon nanotubes at graphitization temperature. *Carbon* 2001;39(11):1681–7.
- [28] Esawi AMK, El Borady MA. Carbon nanotube-reinforced aluminium strips. *Compos Sci Technol* 2008;68(2):486–92.
- [29] Esawi AMK, Morsi K, Sayed A, Taher M, Lanka S. Effect of carbon nanotube (CNT) content on the mechanical properties of CNT-reinforced aluminium composites. *Compos Sci Technol* 2010;70(16):2237–41.
- [30] Hosford WF. *Mechanical behavior of materials*. 1st ed. New York: Cambridge University Press; 2005. p. 381–2.
- [31] Nardone VC, Prewo KM. On the strength of discontinuous silicon carbide reinforced aluminum composites. *Scr Metall* 1986;20(1):43–8.
- [32] Jung HK, Cheong YM, Ryu HJ, Hong SH. Analysis of anisotropy in elastic constants of SiCp/2124 Al metal matrix composites. *Scr Mater* 1999;41(12):1261–7.
- [33] Jeong YJ, Cha SI, Kim KT, Lee KH, Mo CB, Hong SH. Synergistic strengthening effect of ultrafine-grained metals reinforced with carbon nanotubes. *Small* 2007;3(5):840–4.
- [34] Deng CF, Zhang XX, Wang DZ, Lin Q, Li AB. Preparation and characterization of carbon nanotubes / aluminum matrix composites. *Mater Lett* 2007;61(8–9):1725–8.